Article

Thermodynamic and Kinetic Effects of Quaternary Ammonium and Phosphonium Ionic Liquids on CO_2 Hydrate Formation

Lanyun Wang, Yu Chen, Yongliang Xu,* Yajuan Zhang,* Yao Li, Yan Wang, Jianping Wei, and Tingxiang Chu

Read Online

ACCESS | Metrics & More | Article Recommendations

ABSTRACT: The paper elaborates the effects of ionic liquids (ILs) on the phase equilibrium temperature, induction time, gas consumption, gas consumption rate, and water to hydrate conversion in the presence of 0.25, 0.63, 0.95, 1.25, 3.75, 6.25, and 10.00 wt % ethyltributylphosphonium hexafluorophosphate ($[P_{2\ 4\ 4\ 4}][PF_6]$), tributylhexylphosphonium hexafluorophosphate ($[P_{6\ 4\ 4\ 4}][PF_6]$), tetraethylammonium bromide ($[N_{2\ 2\ 2\ 2}]Br$), tetraethylammonium bistrifluoromethanesulfonimide ($[N_{2\ 2\ 2\ 2}]$-$[NTf_2]$), and tetraethylammonium hexafluorophosphate ($[N_{2\ 2\ 2\ 2}][PF_6]$) under a pressure of 2 MPa. The results indicate that all five ILs could increase CO_2 consumption and enhance the water to hydrate conversion. Compared with the pure water system, $[P_{2\ 4\ 4\ 4}][PF_6]$ and $[P_{6\ 4\ 4\ 4}][PF_6]$ shifted the phase equilibrium temperature of CO_2 hydrates to a slightly higher temperature with reduced induction times by boosting CO_2 hydrate nucleation, showing the dual function promotion effects. In contrast, $[N_{2\ 2\ 2\ 2}]Br$, $[N_{2\ 2\ 2\ 2}][NTf_2]$, and $[N_{2\ 2\ 2\ 2}][PF_6]$ shifted the phase equilibrium temperature of CO_2 hydrates to a lower temperature and prolonged the induction time by slowing down CO_2 hydrate nucleation. The inhibition effects of anions on CO_2 hydrates follow an order of $Br^- > [NTf_2]^- > [PF_6]^-$. Besides, the density functional theory and molecular dynamic calculations were conducted to explain the inconsistent influences of $[N_{2\ 2\ 2\ 2}]Br$ and $[N_{4\ 4\ 4\ 4}]Br$ on CO_2 hydrate formation. It was found that the anion−cation interaction of $[N_{2\ 2\ 2\ 2}]Br$ was stronger than that of $[N_{4\ 4\ 4\ 4}]Br$, and Br^- in $[N_{2\ 2\ 2\ 2}]Br$ is less likely to participate in the formation of hydrate cages in the $[N_{2\ 2\ 2\ 2}]Br + H_2O + CO_2$ system according to the intermolecular anion−water, anion−CO_2, and water−water radial distribution function in $[N_{2\ 2\ 2\ 2}]Br + H_2O + CO_2$ and $[N_{4\ 4\ 4\ 4}]Br + H_2O + CO_2$ systems.
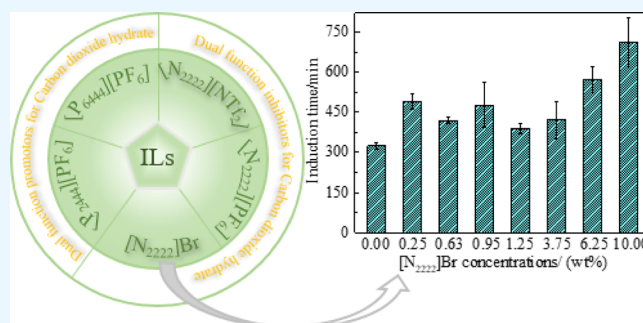
1. INTRODUCTION

The combustion of fossil fuels is the main contributor to elevated CO_2 concentrations in the atmosphere, as well as the main anthropogenic contributor.[1] Carbon dioxide has been identified as the main greenhouse gas causing global warming. In order to prevent the disaster consequences caused by global warming, the world has jointly promoted carbon capture and storage technology.[2] Carbon capture and storage technology refers to the process of separating carbon dioxide from the flue gas generated by fossil fuel combustion, transporting it to a designated place for storage, and isolating it from the atmosphere for a long time.[3] Storing fixed carbon dioxide in the form of hydrates is a powerful measure to reduce the greenhouse effect.[4] Gas hydrate separation is a gas separation and capture technology developed in recent years, which has broad application prospects.[5−8] Natural gas hydrate is a clathrate crystal compound formed by guest molecules (such as CH_4, CO_2, etc.) and host water molecules at low temperatures and high pressures, whereby the host water molecules form polyhedral cavities through hydrogen bonds to envelope the guest molecules in.[9−11] The more popular method is to add chemical additives to reduce the surface tension of the gas−liquid interface and change the microstructure of the liquid, so as to promote the rapid and efficient formation of hydrates and store more gas.[12−15]

Ionic liquids (ILs) have attracted extensive attention due to their excellent properties such as extremely low vapor pressure, high thermal stability, and adjustable ionic and anion structure.[16] In recent years, ILs have been proved by experiments to promote the formation of CO_2 hydrates. Li et al.[17] reported the effects of ILs containing multivariate rings (i.e., 1-(3-sulfonyl) propyl-3-methylimidazole dodecyl sulfonate ([MIMPS][DBSA]), 1-(3-sulfonic acid) propyl piperidine
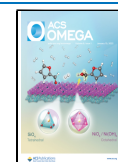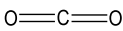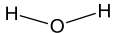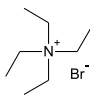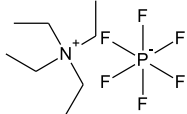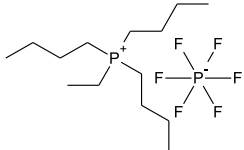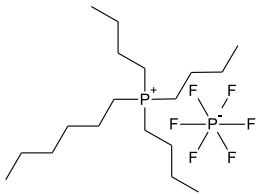
Table 1. Experimental Materials Used in This Work

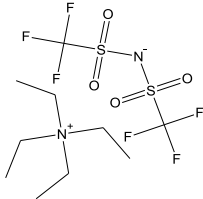| symbol	CAS No	chemical name	purity	chemical structure	supplier
CO_2	124-38-9	Carbon dioxide	≥99.9% (vol%)		Zhengzhou Ruian Gas Technology Co., Ltd.
H_2O	7732-18-5	Deionized water	Deionized		Jiaozuo Xinbolong Co., Ltd.
$[N_{2\,2\,2\,2}]Br$	71-91-0	Tetraethylammonium bromide	≥99.9% (mass fraction)		Qingdao Orike New Material Technology Co., Ltd.
$[N_{2\,2\,2\,2}][NTf_2]$	161401-26-9	Tetraethylammonium bistrifluoromethanesulfonimide	≥99.9% (mass fraction)		Qingdao Orike New Material Technology Co., Ltd.
$[N_{2\,2\,2\,2}][PF_6]$	429-07-2	Tetraethylammonium hexafluorophosphate	≥99.9% (mass fraction)		Qingdao Orike New Material Technology Co., Ltd.
$[P_{2\,4\,4\,4}][PF_6]$	910226-51-6	Ethyltributylphosphonium hexafluorophosphate	≥99.9% (mass fraction)		Qingdao Orike New Material Technology Co., Ltd.
$[P_{6\,4\,4\,4}][PF_6]$	1049619-53-5	Tributylhexylphosphonium hexafluorophosphate	≥99.9% (mass fraction)		Qingdao Orike New Material Technology Co., Ltd.

dodecylbenzene sulfonate ([PIPS][DBSA]), and 1-(3-sulfonic acid) propylpyrrolidine dodecylbenzene sulfonate ([PYPS]-[DBSA])) on the CO_2 hydrate formation. The results show that these solutions not only can reduce the phase equilibrium pressure of CO_2 hydrates but also can increase the CO_2 gas consumption. It may be that multicomponent cyclic cations act as a template for the construction of hydrate cages. Chen et al.[18] found that the consumption of CO_2 increased with the increased concentration of 1-butyl-3-methylimidazolium tetra-fluoroborate ([C_4mim][BF_4]) in forming hydrates. Shin et al.[19] investigated the kinetics of gas hydrate formation in the presence of hydroxyethyl-methyl-morpholinium chloride ([HEMM]Cl), showing that a small amount of [HEMM]Cl (20−20,000 ppm) enhanced the CH_4 hydrate formation. Some tetrabutylammonium and tetrabutyl phosphonium ILs were reported to be able to thermodynamically promote gas hydrate
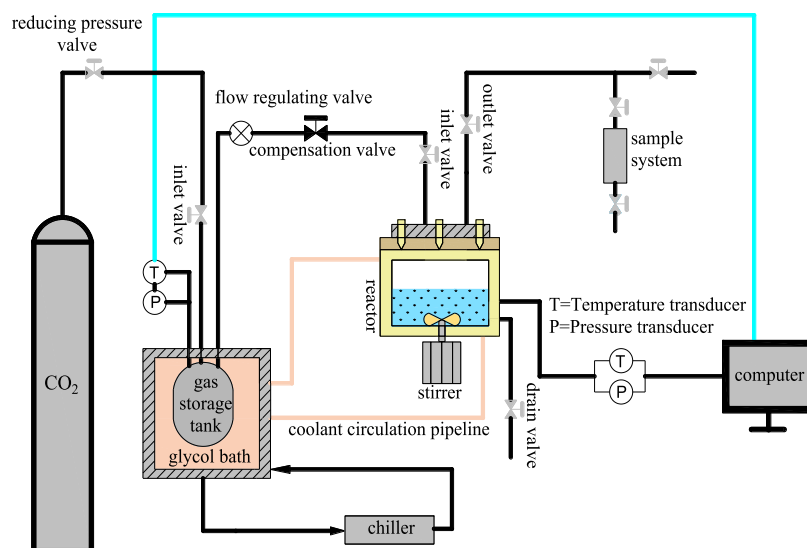
Figure 1. Schematic diagram of the experimental apparatus.

formation.[20−23] $[N_{4\ 4\ 4}]$Br can shfit the temperature and pressure of CO_2 hydrates, possibly because it participates in the construction of hydrate crystal structure.[4] Adding $[N_{4\ 4\ 4}]$Br can reduce the formation pressures of hydrates by approximately 80%.[24] When the $[N_{4\ 4\ 4}]$Br concentration increases, the CO_2 hydrate stability zone was enlarged.[25,26] Its phosphonium analogue, $[P_{4\ 4\ 4}]$Br, has also received attention in CO_2 hydrate formation.[27] The CO_2 gas consumption in $[P_{4\ 4\ 4}]$Br solution is higher than that in $[N_{4\ 4\ 4}]$Br with 1.00 mol % concentration at 275.15 K.[28] Nadia Mayoufi stated that mixed $[P_{4\ 4\ 4}]$Br + CO_2 hydrates can store large amounts of CO_2 and thus could be attractive for gas capture and storage applications.[29]

However, the influence of the ammonium and phosphonium ILs on CO_2 hydrate formation depends on the alkyl chain length, anion structure, and the functional groups. It was reported that the hydroxylation of the alkyl side chain on the cation plays an inhibition role in CH_4 hydrate formation.[30] Tariq et al.[31] reported that the hydroxyl-functionalized ammonium ones, i.e., choline butyrate, choline iso-butyrate, choline hexanoate, and choline octanoate, exhibited dual functionally inhibitory effects on CH_4 hydrate formation. In addition, CO_2 hydrates were inhibited more strongly with the increasing concentration of tetramethylammonium chloride ($[N_{1\ 1\ 1}]$Cl), tetraethylammonium hydroxide ($[N_{2\ 2\ 2}]$-[OH]), and tetrapropylammonium hydroxide ($[N_{3\ 3\ 3}]$-[OH]).[32] These results show that the presence of hydroxyl groups in the IL structure could strengthen the hydrogen bonding between ILs and water, resulting in the destruction of hydrogen bonds between water molecules and thus effectively inhibiting the hydrate formation.[33,34]

Nevertheless, there are still few data on the effect of ILs on hydrate formation.[35] Previous studies on the effects of quaternary ammonium and quaternary phosphine ILs on hydrate formation mainly focused on $[N_{4\ 4\ 4}]$Br and $[P_{4\ 4\ 4}]$Br. Here, three tetraethylammonium ILs, tetraethylammonium bromide ($[N_{2\ 2\ 2}]$Br), tetraethylammonium bistrifluoromethanesulfonimide ($[N_{2\ 2\ 2}][NTf_2]$), and tetraethylammonium hexafluorophosphate ($[N_{2\ 2\ 2}][PF_6]$), and two quaternary phosphonium hexafluorophosphate ILs with different lengths of cationic alkyl side chains, ethyltributylphosphonium hexafluorophosphate ($[P_{2\ 4\ 4}][PF_6]$) and

tributylhexylphosphonium hexafluorophosphate ($[P_{6\ 4\ 4}]$-[PF_6]), will be applied to affect CO_2 hydrate formation. In this work, the thermodynamic and kinetic characteristics of CO_2 hydrate formation will be measured and discussed by analyzing the phase equilibrium temperatures, induction times, gas consumptions, gas consumption rates, and water to hydrate conversions.

2. EXPERIMENTAL SECTION

2.1. Experimental Materials. Table 1 shows the symbols, chemical names, purities, chemical structures, and suppliers of the experimental materials used here. $[N_{2\ 2\ 2}]$Br is soluble in water with a solubility of about 3.152 g/g H_2O (298.15 K),[36] while other ILs are insoluble in water under the experimental conditions. IL concentrations of 0.25, 0.63, 0.95, 1.25, 3.75, 6.25, and 10.00 wt % are prepared for each experimental set.

2.2. Experimental Apparatus. The schematic diagram of the experimental apparatus for generating CO_2 hydrates is shown in Figure 1, and the physical picture of the experimental apparatus is shown in Figure 2. It mainly consists of a visual cylindrical high-pressure reactor, a magnetic stirrer, a chiller, and a gas storage tank. The visual cylindrical high-pressure reactor of 100 mL can withstand a maximum pressure of 20 MPa. The magnetic stirrer can reach a maximum speed of

Figure 2. Physical picture of the experimental apparatus for gas hydrate formation.

1500 rpm. The chiller is used to cool the agitation reactor through circulating a coolant within a temperature range of 258.15~378.15 K. The gas storage tank is submerged into the glycol cooling bath to pre-cool the inputting gas. An automatic gas compensation valve (S115121-NC, Shenzhen Siteke Pneumatic Hydraulic Co., Ltd.) is employed to adjust the pressure in the reactor to be about 2 MPa. The temperature transducers (Pt-100 thermocouple) and pressure transducers (HQ-1000), with an uncertainty of 0.01 K and 0.01 MPa, respectively, are used to measure the temperature and pressure of the high-pressure reactor and the gas storage tank during the experiments. All materials are weight by an electronic balance with an uncertainty of 0.1 mg.

2.3. Experimental Procedure. Before the experiment, 55 mL of deionized water was measured by a graduated cylinder so that the gas−liquid interface of the reactor was located in the visible range. The electronic balance was used to weigh ILs with different mass fractions, then poured them into a beaker, and mixed with deionized water evenly. The sample systems containing different concentrations of ILs were prepared. The air tightness of the autoclave needed to be checked to ensure that the system was well sealed. The reactor was washed with deionized water three times, and then, the prepared sample was loaded into the reactor after drying. The reactor was purged with 0.1 MPa CO_2 gas after sealing it, and then, the pressure was released. This operation was repeated three times to remove the residual air. The cooling reactor was driven by a chiller that lowered the temperature of the glycol bath at a cooling rate of 1 K/h. Afterward, the reactor was pressurized with CO_2 to 2 MPa, and the pressure compensation valve was opened to keep the pressure in the reactor constant during the experiment. When the temperature of the reactor was steady, the magnetic stirrer was opened at a speed of 800 rpm.[37] The data acquisition system was then switched on to record the temperature and pressure inside the reactor, and the experiment started. The reaction was accomplished when the pressure in the gas storage tank no longer dropped and CO_2 hydrates were fully formed. To ensure the accuracy and reproducibility of the experimental results, each experiment should be repeated at least three times.

2.4. Calculation Methods. *2.4.1. Gas Consumption.* Gas consumption (n_t) is defined as the millimole of gas consumed per mole of water, and the expression is shown as eq 1.[38]

$$n_t = \frac{1000 \times \Delta n_t}{n_{H_2O}} \tag{1}$$

where n_{H_2O} represents the initial number of moles of water; Δn_t is the mole of gas consumption at time t, which is calculated from eq 2.

$$\Delta n_t = \left(\frac{PV}{ZRT}\right)_0 - \left(\frac{PV}{ZRT}\right)_t \tag{2}$$

where V, P, and T are the volume, pressure, and temperature of the gas storage tank, respectively; Z stands for the gas compressibility factor obtained from the Peng-Robinson state equation;[39] R is the universal gas constant; the subscripts 0 and t represent the reaction time of 0 and t minutes, respectively.

2.4.2. Gas Consumption Rate. The gas consumption rate represents millimole CO_2 per mole of water per unit time and is calculated by eq 3.

$$v_t = \left(\frac{dn_t}{dt}\right) = \frac{n_{t,t+\Delta t} - n_{t,t}}{\Delta t} \tag{3}$$

where v_t is the gas consumption rate at time t; $n_{t,t+\Delta t}$ and $n_{t,t}$ are gas consumption at time $t + \Delta t$ and t, respectively; Δt is the time step.

2.4.3. Water to Hydrate Conversion. Water to hydrate conversion is defined as the mole number of water converted to the hydrate per mole of feed water, as shown in eq 4.

$$conversion = \frac{M \times n_t}{n_{H_2O}} \tag{4}$$

where M is the hydration number. CO_2 gas forms simple hydrates with structure I (sI), and the expression of M for simple sI hydrates is shown in eq 5.[9]

$$M = \frac{46}{6\theta_L + \theta_S} \tag{5}$$

where θ_L and θ_S are the fractional occupancies of large pores and small pores, respectively, and are calculated by eq 6.

$$\theta_i = \frac{C f_{CO_2}}{1 + C f_{CO_2}} \tag{6}$$

In this equation, f_{CO_2} represents the fugacity of CO_2 in the gas phrase; C_i is the Langmuir constant[40,41] of CO_2 in type i cavity and is formulated as eq 7:

$$C_i = \frac{A_i}{T} \exp\left(\frac{B_i}{T}\right) \tag{7}$$

where A_i and B_i are constants,[42] for small cavities: $A_i = 2.474 \times 10^{-4}$ K/atm, $B_i = 3410$ K; for large cavities: $A_i = 4.246 \times 10^{-2}$ K/atm, $B_i = 2813$ K. The fugacity of the pure component is calculated using eq 8.[39]

$$\ln\frac{f}{p} = Z - 1 - \ln(Z - B) - \frac{A}{2\sqrt{2}B}\ln\left(\frac{Z + 2.414B}{Z - 0.414B}\right) \tag{8}$$

$$A = \frac{a(T)P}{R^2T^2}; \quad B = \frac{bP}{RT} \tag{9}$$

$$a(T) = a(T_c) \times a(T_r, \omega); \quad b(T) = b(T_c) \tag{10}$$

$$a(T_c) = 0.45724\frac{R^2T_c^2}{P_c}; \quad b(T_c) = 0.07780\frac{RT_c}{P_c} \tag{11}$$

$$a(T_r, \omega) = [1 + (0.37464 + 1.54226\omega - 0.26992\omega^2)(1 - T_r^{0.5})]^2 \tag{12}$$

$$T_r = \frac{T}{T_c} \tag{13}$$

where T_c and P_c are the critical temperature and pressure of CO_2:[43] $T_c = 304.12$ K, $P_c = 73.74$ bar; ω is the eccentricity factor of CO_2, $\omega = 0.225$; T_r is the contrast temperature.

3. RESULTS AND DISCUSSION

3.1. $P-T-t$ Curves of CO_2 Hydrate Formation. Figure 3 shows the typical $P-T-t$ curves of CO_2 hydrate formation in the presence of ILs (0.25 wt % $[N_{2\,2\,2}]NTf_2$) under a
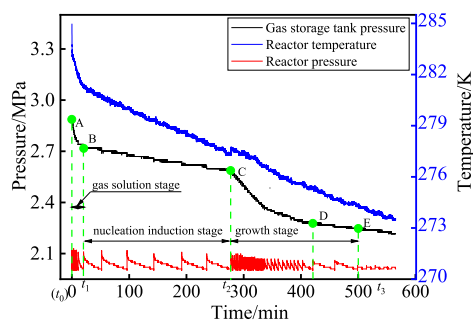
Figure 3. $P-T-t$ variation curves in the process of CO_2 hydrate formation at 2 MPa in the $[N_{2\,2\,2\,2}][NTf_2] + CO_2 + H_2O$ system.

constant pressure of 2 MPa. It is observed that the pressure of the gas storage tank dropped rapidly due to the continuous dissolution of gas in the solution during the t_0-t_1 stage (i.e., gas dissolution stage). Meanwhile, the temperature of the stirred reactor decreased dramatically by the cooling effect of the circulating coolant. In the t_1-t_2 stage (i.e., nucleation induction stage), CO_2 in the solution became saturated, and the pressure of the gas storage tank and the temperature of the reactor both showed a linear and slow downward trend. At time t_2, the reaction system enters the hydrate growth stage, and the temperature and pressure here are defined as the phase equilibrium temperature and pressure. The pressure of the gas storage tank decreased frequently, and the pressure of the

Table 2. Experimental Results of CO_2 Hydrate Formation in the Presence of Ammonium and Phosphonium ILs under 2 MPa[a]

exp. no.	experimental system	T_{eq} (K) (±stdev)	induction time (min) (±stdev)	gas consumption (mmol CO_2/mol H_2O) (±stdev)	water to hydrate conversion (%) (±stdev)
1	pure water	276.25(±0.68)	324(±13)	37.32(±2.56)	27.56(±0.43)
2	0.25 wt % $[N_{2\,2\,2\,2}]Br + CO_2 + H_2O$	274.45(±0.37)	491(±29)	43.29(±1.52)	31.53(±0.75)
3	0.63 wt % $[N_{2\,2\,2\,2}]Br + CO_2 + H_2O$	275.55(±0.42)	420(±12)	54.93(±4.90)	41.10(±2.00)
4	0.95 wt % $[N_{2\,2\,2\,2}]Br + CO_2 + H_2O$	273.45(±0.63)	477(±83)	43.70(±5.77)	31.79(±2.34)
5	1.25 wt % $[N_{2\,2\,2\,2}]Br + CO_2 + H_2O$	276.15(±0.18)	390(±19)	51.61(±0.58)	37.86(±0.24)
6	3.75 wt % $[N_{2\,2\,2\,2}]Br + CO_2 + H_2O$	275.65(±0.32)	422(±70)	50.64(±9.15)	36.51(±3.21)
7	6.25 wt % $[N_{2\,2\,2\,2}]Br + CO_2 + H_2O$	273.25(±0.54)	572(±48)	47.36(±10.83)	35.02(±3.56)
8	10.00 wt % $[N_{2\,2\,2\,2}]Br + CO_2 + H_2O$	270.65(±0.65)	712(±90)	42.88(±5.25)	31.42(±2.12)
9	0.25 wt % $[N_{2\,2\,2\,2}][NTf_2] + CO_2 + H_2O$	273.35(±0.62)	569(±52)	40.18(±3.64)	29.53(±0.63)
10	0.63 wt % $[N_{2\,2\,2\,2}][NTf_2] + CO_2 + H_2O$	275.65(±0.20)	350(±15)	48.03(±1.27)	35.51(±0.11)
11	0.95 wt % $[N_{2\,2\,2\,2}][NTf_2] + CO_2 + H_2O$	273.45(±0.58)	532(±63)	41.60(±1.82)	30.12(±0.77)
12	1.25 wt % $[N_{2\,2\,2\,2}][NTf_2] + CO_2 + H_2O$	275.35(±0.31)	414(±59)	47.65(±1.75)	34.95(±0.51)
13	3.75 wt % $[N_{2\,2\,2\,2}][NTf_2] + CO_2 + H_2O$	273.95(±0.12)	541(±20)	44.70(±1.07)	32.08(±0.37)
14	6.25 wt % $[N_{2\,2\,2\,2}][NTf_2] + CO_2 + H_2O$	274.02(±0.54)	514(±98)	43.62(±0.49)	31.66(±0.23)
15	10.00 wt % $[N_{2\,2\,2\,2}][NTf_2] + CO_2 + H_2O$	273.05(±0.24)	529(±73)	38.29(±8.59)	28.98(±2.87)
16	0.25 wt % $[N_{2\,2\,2\,2}][PF_6] + CO_2 + H_2O$	272.75(±0.14)	584(±30)	37.89(±4.47)	27.95(±1.42)
17	0.63 wt % $[N_{2\,2\,2\,2}][PF_6] + CO_2 + H_2O$	276.15(±0.50)	389(±12)	44.21(±5.25)	32.09(±1.87)
18	0.95 wt % $[N_{2\,2\,2\,2}][PF_6] + CO_2 + H_2O$	272.95(±0.63)	590(±65)	39.21(±3.18)	28.66(±1.29)
19	1.25 wt % $[N_{2\,2\,2\,2}][PF_6] + CO_2 + H_2O$	276.25(±0.67)	355(±33)	42.71(±0.16)	30.79(±0.24)
20	3.75 wt % $[N_{2\,2\,2\,2}][PF_6] + CO_2 + H_2O$	275.45(±0.48)	396(±48)	41.41(±3.89)	29.63(±0.66)
21	6.25 wt % $[N_{2\,2\,2\,2}][PF_6] + CO_2 + H_2O$	275.15(±0.27)	365(±21)	40.17(±5.61)	28.84(±1.55)
22	10.00 wt % $[N_{2\,2\,2\,2}][PF_6] + CO_2 + H_2O$	274.85(±0.62)	406(±30)	36.43(±8.61)	26.86(±2.56)
23	0.25 wt % $[P_{2\,4\,4\,4}][PF_6] + CO_2 + H_2O$	273.95(±0.72)	495(±43)	53.23(±2.21)	38.57(±0.62)
24	0.63 wt % $[P_{2\,4\,4\,4}][PF_6] + CO_2 + H_2O$	276.35(±0.11)	362(±35)	55.75(±1.98)	40.02(±0.15)
25	0.95 wt % $[P_{2\,4\,4\,4}][PF_6] + CO_2 + H_2O$	275.35(±0.71)	393(±26)	51.15(±6.65)	37.44(±1.72)
26	1.25 wt % $[P_{2\,4\,4\,4}][PF_6] + CO_2 + H_2O$	276.15(±0.29)	303(±48)	54.20(±4.02)	39.01(±1.38)
27	3.75 wt % $[P_{2\,4\,4\,4}][PF_6] + CO_2 + H_2O$	276.95(±0.48)	265(±27)	64.63(±4.93)	47.50(±1.46)
28	6.25 wt % $[P_{2\,4\,4\,4}][PF_6] + CO_2 + H_2O$	277.05(±0.39)	284(±14)	70.04(±5.22)	51.86(±1.58)
29	10.00 wt % $[P_{2\,4\,4\,4}][PF_6] + CO_2 + H_2O$	277.15(±0.50)	260(±58)	67.61(±4.93)	48.08(±1.49)
30	0.25 wt % $[P_{6\,4\,4\,4}][PF_6] + CO_2 + H_2O$	273.65(±0.52)	526(±58)	49.10(±4.44)	35.99(±0.64)
31	0.63 wt % $[P_{6\,4\,4\,4}][PF_6] + CO_2 + H_2O$	276.75(±0.40)	285(±30)	51.40(±0.88)	37.77(±0.34)
32	0.95 wt % $[P_{6\,4\,4\,4}][PF_6] + CO_2 + H_2O$	274.65(±0.12)	435(±54)	47.55(±3.86)	34.87(±0.74)
33	1.25 wt % $[P_{6\,4\,4\,4}][PF_6] + CO_2 + H_2O$	276.65(±0.62)	295(±47)	49.88(±1.65)	36.39(±0.79)
34	3.75 wt % $[P_{6\,4\,4\,4}][PF_6] + CO_2 + H_2O$	277.15(±0.60)	255(±56)	63.51(±7.95)	46.34(±2.32)
35	6.25 wt % $[P_{6\,4\,4\,4}][PF_6] + CO_2 + H_2O$	276.95(±0.24)	287(±51)	68.09(±5.96)	48.55(±1.96)
36	10.0 wt % $[P_{6\,4\,4\,4}][PF_6] + CO_2 + H_2O$	276.55(±0.53)	297(±16)	65.18(±0.23)	47.94(±0.18)

[a]Note: T_{eq} refers to the phase equilibrium temperature when CO_2 hydrates are generated. The value of each parameter represents the average value of the repeated systems, and the parameter variations of the repeated systems are determined by calculating the standard deviation of the data and reflect the degree of dispersion of repeated experiments.
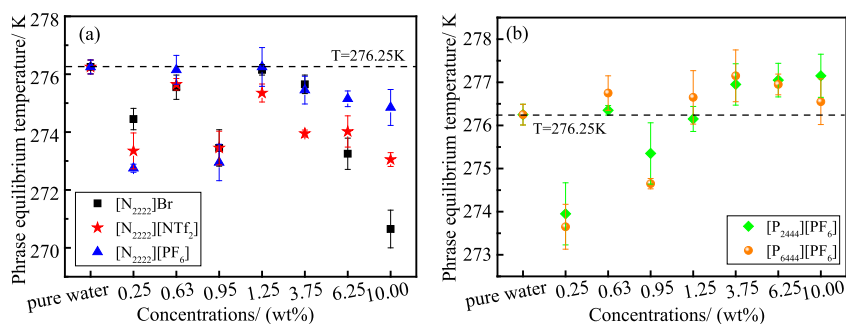
Figure 4. CO_2 hydrate phase equilibrium temperature scatter diagrams of IL samples with different concentrations at 2 MPa. (a) $[N_{2\,2\,2\,2}]Br/$ $[N_{2\,2\,2\,2}][NTf_2]/[N_{2\,2\,2\,2}][PF_6]$ and (b) $[P_{2\,4\,4\,4}][PF_6]/[P_{6\,4\,4\,4}][PF_6]$. The dotted line in the figure denotes the phase equilibrium temperature of the pure water system, which is 276.15 K.

reactor changes rapidly, while the temperature in the reactor rose sharply (about 0.5 K) which can be see from the blue curve, which indicates that a large number of CO_2 hydrates were generated instantly. This is due to a factor that the hydration process is an exothermic reaction, and the reaction heat cannot be removed immediately, which leads to a increase of temperature. The CD section is the rapid growth stage, and after point D, the hydrate formation rate was slowed down. Also, the pressure dropping rate gradually decreased over time. After time t_3, the pressure decrease of the gas storage tank tended to be constant, indicating that the hydrate reaction was completed and the experiment was over.

3.2. Phase Equilibrium Temperature. The equilibrium temperatures, induction times, gas consumptions, and water to hydrate conversions during CO_2 hydrate formation in the presence of ammonium and phosphonium ILs are included in Table 2. Each parameter variation is expressed by error bar representing the standard deviation of the data in the following figures.

In order to determine the effect of the concentration and type of IL on the phase equilibrium temperature of CO_2 hydrates, the phase equilibrium temperature scatter diagrams of ILs + CO_2 + H_2O systems with various concentrations are shown in Figure 4. The phase equilibrium temperature of CO_2 hydrates was reported to be 277.4 K at 1.85MPa,[32] and 276.5 K was reported in another paper.[44] Within the error allowed, the phase equilibrium conditions in the pure water system in this work were close to the data reported by Seo[45] which are 277.16 K at 2 MPa, which also confirmed the reliability of the experiment equipment and experimental method adopted in this work. Figure 4a presents the phase equilibrium temperatures of CO_2 hydrates in the presence of $[N_{2\,2\,2\,2}]Br$, $[N_{2\,2\,2\,2}][NTf_2]$, and $[N_{2\,2\,2\,2}][PF_6]$ with concentrations of 0.25, 0.63, 0.95, 1.25, 3.75, 6.25, and 10.00 wt %. As noticed in Figure 4, the phase equilibrium temperatures of all ammonium IL systems are lower than that of the pure water system (276.25 K), indicating that $[N_{2\,2\,2\,2}]Br$, $[N_{2\,2\,2\,2}][NTf_2]$, and $[N_{2\,2\,2\,2}][PF_6]$ make thermodynamic inhibition roles, shifting the phase equilibrium temperature of CO_2 hydrates to lower temperatures. When the concentration of $[N_{2\,2\,2\,2}]Br$ is less than 1 wt %, the phase equilibrium temperature fluctuates and there are no obvious changing regularities. However, when the concentration is greater than 1 wt %, the phase equilibrium temperature decreases with an increase of $[N_{2\,2\,2\,2}]Br$ concentration. This also occurs in the case of $[N_{2\,2\,2\,2}][NTf_2]$ and $[N_{2\,2\,2\,2}][PF_6]$ with a concentration of lower than 1 wt %. It is worth noting that when the concentration is greater than 1

wt %, the differences of the phase equilibrium temperature of three ammonium IL systems gradually expand. Under a pressure of 2 MPa, the phase equilibrium temperatures of CO_2 hydrates in the presence of 10.00 wt % $[N_{2\,2\,2\,2}]Br$, $[N_{2\,2\,2\,2}][NTf_2]$, and $[N_{2\,2\,2\,2}][PF_6]$ are reduced by 5.60, 3.20, and 1.40 K, respectively. Arguably, the anions do affect the thermodynamic inhibition on CO_2 hydrates and conform to an order of $Br^- > [NTf_2]^- > [PF_6]^-$ with the same cation. This indicates that the inhibitory effect increased as anion size decreased or anion charge density increased.[46] Thus, the presence of Br^- results in increasing electrostatic and van der Waals interactions between IL and water molecules, which leads to a shift in the hydrate phase equilibrium curves to low temperatures. The results are also consistent with the inhibitory effect of several imidazolium ILs reported by Xiao et al.,[47] stating that a single halide anion has stronger ability to form a hydrogen bond with water which has greater chance to disrupt the hydrogen bonding between water molecules. Therefore, $[N_{2\,2\,2\,2}]Br$ has great application potential in hydrate inhibition and should be paid more attention in the future work.

The phase equilibrium temperatures of $[P_{2\,4\,4}][PF_6]/$ $[P_{6\,4\,4\,4}][PF_6]$ + CO_2 + H_2O systems are shown in Figure 4b. There are no significant differences in the phase equilibrium temperatures between $[P_{2\,4\,4}][PF_6]$ and $[P_{6\,4\,4\,4}][PF_6]$ systems for all concentrations. Except in the presence of 0.25 and 0.95 wt % phosphonium ILs, the phase equilibrium temperatures of CO_2 hydrates after adding $[P_{2\,4\,4\,4}][PF_6]$ and $[P_{6\,4\,4\,4}][PF_6]$ are slightly higher than those of the pure water system. When the concentrations are larger than 1 wt %, increasing the $[P_{2\,4\,4\,4}][PF_6]$ and $[P_{6\,4\,4\,4}][PF_6]$ concentration makes no significant change to the phase equilibrium temperatures. The phase equilibrium temperatures of CO_2 hydrates of 10.00 wt % $[P_{2\,4\,4\,4}][PF_6]$ and $[P_{6\,4\,4\,4}][PF_6]$ systems only increased by 0.90 and 0.30 K, respectively. However, increasing the concentration of phosphonium ILs, the equilibrium temperatures are not decreased, indicating that the two phosphonium ILs are more favorable for the thermodynamic formation of CO_2 hydrates compared to the ammonium congeners which lowered the equilibrium temperatures with higher concentrations. This may be because $[P_{2\,4\,4\,4}][PF_6]$ and $[P_{6\,4\,4\,4}][PF_6]$ have longer alkyl chains. Xiao[47] and Chu et al.[48] found that the increase of alkyl chain length would weaken the inhibition effect on the hydrate formation. In the presence of $[N_{4\,4\,4}]Br^{[25,49,50]}$ and $[P_{4\,4\,4}Br]$,[51−53] signifcant improvement occurred in the conditions of CO_2 hydrate formation. Phosphonium-based ILs
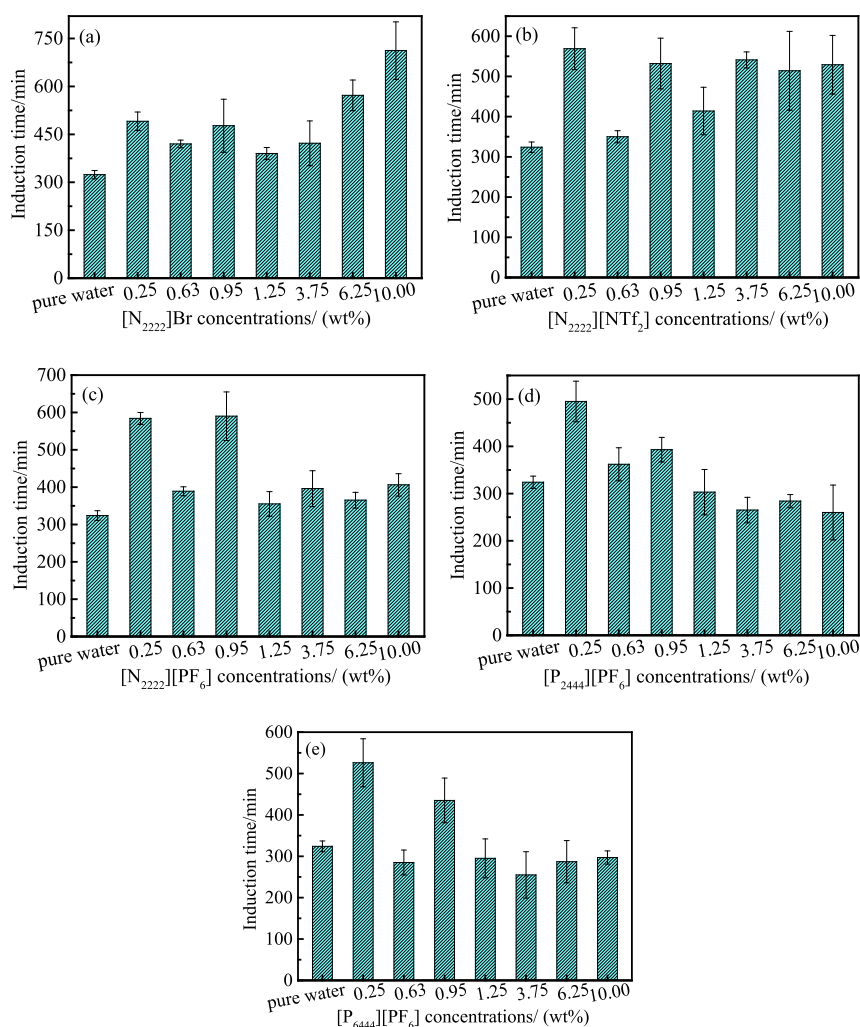
Figure 5. Influence of IL concentration on induction time at 2 MPa, (a) $[N_{2\,2\,2\,2}]Br$, (b) $[N_{2\,2\,2\,2}][NTf_2]$, (c) $[N_{2\,2\,2\,2}][PF_6]$, (d) $[P_{2\,4\,4\,4}][PF_6]$, and (e) $[P_{6\,4\,4\,4}][PF_6]$.

showed less steric effect and higher charge transfer and cation−anion interaction energy than ammonium-based ILs.[54] This may lead to the formation of semi-cage hydrates in the presence of phosphonium-based ILs, more stable spatial structure, and better thermodynamic promotion effect.

3.3. Induction Time.
Induction time is an important evaluation index of formation kinetics of gas hydrates, indicating the speed of hydrate nucleation. The induction time is defined as the time interval from the beginning of the reaction to the sudden increase of the temperature in the high-pressure reactor, which can be determined from the $P−T−t$ curve. Figure 5 shows the induction times of CO_2 hydrate formation in the systems of IL + CO_2 + H_2O with different concentrations under 2 MPa.

In Figure 5a, the induction times of CO_2 hydrate formation of 0.25, 0.63, 0.95, 1.25, 3.75, 6.25, and 10.00 wt % $[N_{2\,2\,2\,2}]Br$ aqueous solutions were 491, 420, 477, 390, 422, 572, and 712 min, respectively. Compared with the pure water system (324 min), the induction time increased by 51.54, 29.63, 47.22, 20.37, 30.25, 76.54, and 119.75%, respectively. This implies that $[N_{2\,2\,2\,2}]Br$ can be used as a kinetic inhibitor to delay the nucleation of CO_2 hydrates. Furthermore, the concentration of ILs is an important factor affecting the induction time. When the added $[N_{2\,2\,2\,2}]Br$ concentration is less than 1 wt %, there

was no obvious correlation between the concentration of ILs and the induction time. However, when the concentration was greater than 1 wt %, the induction time was prolonged with the increase of concentration, which indicates that for the range of 1.25 wt % $\sim$ 10.00 wt %, the large IL concentration inhibits the kinetic formation on CO_2 hydrates.

For $[N_{2\,2\,2\,2}][NTf_2]$ and $[N_{2\,2\,2\,2}][PF_6]$ systems, Figure 5b,c demonstrates that the induction times of all concentration samples are also longer than that of the pure water system, which indicates that both are also kinetic inhibitors. When the concentration was less than 1 wt %, the rule between induction time and concentration was almost the same as $[N_{2\,2\,2\,2}]Br$. However, when the concentration was greater than 1 wt %, the induction time did not improve with the increase of the concentration but fluctuated around a certain value. The reason for this phenomenon may be that $[NTf_2]^{-55}$ and $[PF_6]^{-56}$ are hydrophobic, and both of these ILs exist in solid form in water and cannot be solvated. The number of ions in water does not seem to change greatly with the increase of IL concentration, so the hydrogen bond destruction effect of ILs on the formation of hydrate cages does not change obviously. Therefore, the induction time does not show a significant difference with the increase of concentration. Additionally, the induction times in 0.25 wt % $[N_{2\,2\,2\,2}][NTf_2]$ and

$[N_{2 2 2 2}][PF_6]$ systems were longer than those in 10.00 wt % samples, cations and anions were subjected to the strong force of ionic bonds, and ILs were in the solid state. In addition, because of the asymmetry of the cation and anion, the volume difference is large, so that the freedom of ion movement is relatively high.[57] The higher the concentration, the more hydrate nucleation points and the shorter the induction time, suggesting that the increased nucleation sites may make some compensation for the inhibition effect, allowing that highly concentrated ILs are not advantagous in delaying CO_2 hydrate nucleation.

In Figure 5d, the induction times of 0.25, 0.63, 0.95, 1.25, 3.75, 6.25, and 10.00 wt % $[P_{2 4 4 4}][PF_6]$ systems at 2 MPa were 495, 362, 393, 303, 265, 284, and 260 min, respectively. The rules were consistent with $[N_{2 2 2 2}]Br/[N_{2 2 2 2}]/[NTf_2]/$ $[N_{2 2 2 2}][PF_6]$ when the concentration was less than 1 wt %. Compared with the pure water system, the induction times at 0.25, 0.63, and 0.95 wt % increased by 52.78, 11.73, and 21.30%, respectively, indicating that low concentration $[P_{2 4 4 4}][PF_6]$ inhibited the nucleation of CO_2 hydrates. When the concentration was higher than 1 wt %, the induction time at 1.25, 3.75, 6.25, and 10.00 wt % decreased by 6.48, 18.21, 12.35, and 19.75% compared to the pure water system, respectively, showing that the induction time did not change significantly with the increase of concentration and the formation of CO_2 hydrates was promoted in this concentration range. As expected, the results of $[P_{6 4 4 4}][PF_6]$ were analogous to $[P_{2 4 4 4}][PF_6]$ from Figure 5e.

Figure 6 presents the induction times of five ILs at different concentrations under 2 MPa. The overall observation shows
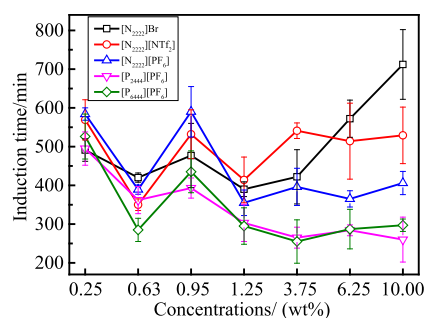

Figure 6. Comparison chart of induction times of five ILs with different concentrations at 2 MPa.

that the induction times of the ammonium IL systems are longer than that of the pure water system, indicating that $[N_{2 2 2 2}]Br$, $[N_{2 2 2 2}][NTf_2]$, and $[N_{2 2 2 2}][PF_6]$ can inhibit the nucleation of CO_2 hydrates. For further analysis, the induction times of the low concentration ammonium IL systems were not much different, and only when the ammonium IL concentration was greater than 3.75 wt %, the induction time was significantly different. For example, when the concentrations of $[N_{2 2 2 2}]Br$, $[N_{2 2 2 2}][NTf_2]$, and $[N_{2 2 2 2}][PF_6]$ were 6.25 and 10.00 wt %, the prolongation effect of anions on induction time decreased in the following order: $Br^- > [NTf_2]^- > [PF_6]^-$. This result clearly justifies that Br^- has the strongest kinetic inhibitory effect on the nucleation of CO_2 hydrates. It has been reported that the inhibition effect of anions on hydrate formation increases with decreasing size or increasing charge density.[46] Therefore, compared with $[NTf_2]^-$ and $[PF_6]^-$, the smallest size and highest charge density Br^- is most conducive to inhibiting the formation of

CO_2 hydrates. By analyzing the phosphonium IL systems, it was found that the induction times with the same concentration of $[P_{2 4 4}][PF_6]$ and $[P_{6 4 4}][PF_6]$ systems were similar and generally lower than that of the pure water system, implying that they had a slight promoting effect on CO_2 hydrate nucleation. Therefore, $[P_{2 4 4}][PF_6]$ and $[P_{6 4 4}][PF_6]$ can promote the formation of hydrates rather than inhibition.

3.4. CO_2 Consumption. Gas consumption is another important parameter of hydrate formation kinetics. In this work, the real-time gas consumption in the hydration process was calculated by the pressure change of CO_2 in the gas storage tank. Figure 7a−e shows the kinetic curves of CO_2 gas consumption of gas hydrate systems in the presence of ILs with different concentrations under 2 MPa within 800 min. As shown in these figures, the CO_2 consumption variation trends of all systems are basically similar, broadly showing the two-stage gas consumption features. In the first stage, the gas consumptions rise almost vertically within 20 min owing to the dissolution of CO_2 in the aqueous systems, and the gas consumption approaches 15 mmol CO_2/mol H_2O. In the second stage, the substantial increase in gas consumption was attributed to the formation and growth of large amounts of hydrates.

As depicted in Figure 7a, the final CO_2 capture values in $[N_{2 2 2 2}]Br$ aqueous solution with concentrations of 0.25, 0.63, 0.95, 1.25, 3.75, 6.25, and 10.00 wt % were 43.29, 54.93, 43.70, 51.61, 50.64, 47.36, and 42.88 mmol CO_2/mol H_2O, respectively. Compared with the pure water system (37.32 mmol CO_2/mol H_2O), the CO_2 consumption increased by 16.00, 47.19, 17.10, 38.29, 35.69, 26.90, and 14.90%, respectively. Apparently, after adding $[N_{2 2 2 2}]Br$, the CO_2 consumptions were greatly enhanced compared to the pure water system, which implied that $[N_{2 2 2 2}]Br$ could improve the CO_2 capture. In Figure 7b,c, CO_2 consumption in $[N_{2 2 2 2}][NTf_2]$ and $[N_{2 2 2 2}][PF_6]$ systems varied with concentration in a similar way to those of $[N_{2 2 2 2}]Br$ systems.

CO_2 consumption of all ammonium IL-containing systems is different and follows an order of 0.63 wt % > 1.25 wt % > 3.75 wt % > 6.25 wt % > 0.95 wt % > 0.25 wt % > 10.00 wt % > pure water. It is clearly seen that the concentration does not have a linear relationship with the final CO_2 consumption. However, in general, CO_2 consumption decreases with the increasing IL concentration, indicating that increasing the concentration of ammonium ILs is not favorable for the formation of CO_2 hydrates, which might be due to the hydrogen bond interaction between the anions and water molecules.

Combined with Table 2 and Figure 7d, it was found that the final CO_2 consumptions of $[P_{2 4 4}][PF_6]$ systems with 0.25, 0.63, 0.95, 1.25, 3.75, 6.25, and 10.00 wt % were 53.23, 55.75, 51.15, 54.20, 64.63, 70.04, and 67.61 mmol CO_2/mol H_2O, respectively. Compared with the pure water system, the CO_2 consumption increased by 42.63, 49.38, 37.58, 45.23, 73.18, 87.67, and 81.16%, respectively. In addition, as Figure 7e shows, CO_2 consumption of $[P_{6 4 4}][PF_6]$ systems changed with concentration with a similar regularity to the $[P_{2 4 4}][PF_6]$ systems. CO_2 consumption of $[P_{2 4 4}][PF_6]/$ $[P_{6 4 4}][PF_6]$ systems followed an order of 6.25 wt % > 10.00 wt % > 3.75 wt % > 0.63 wt % > 1.25 wt % > 0.25 wt % > 0.95 wt % > pure water. The CO_2 consumptions of all phosphonium IL systems were higher than pure water, which indicated that $[P_{2 4 4}][PF_6]$ and $[P_{6 4 4}][PF_6]$ could also
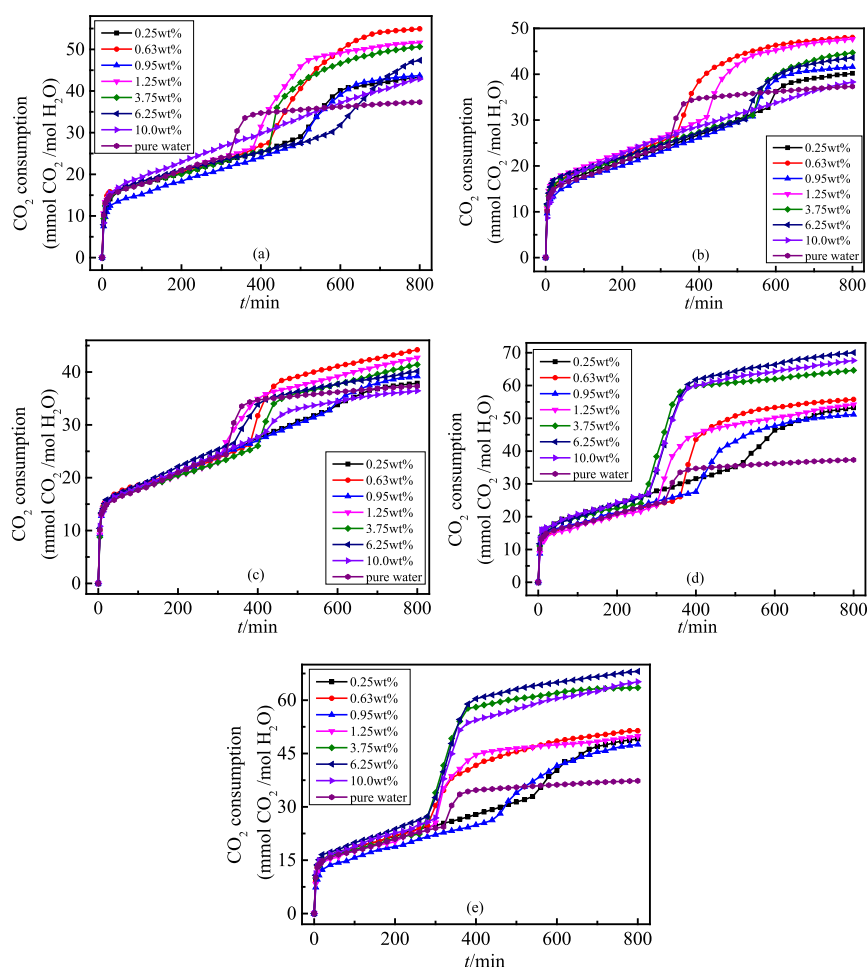
Figure 7. CO_2 real-time gas consumption kinetic curves under different IL concentrations during the formation of CO_2 hydrates at 2 MPa, (a) $[N_{2\,2\,2\,2}]Br$, (b) $[N_{2\,2\,2\,2}][NTf_2]$, (c) $[N_{2\,2\,2\,2}][PF_6]$, (d) $[P_{2\,4\,4\,4}][PF_6]$, and (e) $[P_{6\,4\,4\,4}][PF_6]$.

improve the CO_2 capacity. Different from the ammonium IL systems, high concentration $[P_{2\,4\,4}][PF_6]$ and $[P_{6\,4\,4\,4}][PF_6]$ usually have larger CO_2 consumption, and CO_2 consumptions in the 10.00, 6.25, and 3.75 wt % systems are very close and much higher than those of other concentration systems. This indicates that the high-concentration phosphonium IL system was more conducive to CO_2 absorption.

The final CO_2 consumptions of the different IL systems are shown in Figure 8. The gas consumptions of ammonium IL systems with the same concentration are close, and the influencing order of anions on CO_2 consumption followed an order of $Br^- > [NTf_2]^- > [PF_6]^-$. Besides, the $[P_{2\,4\,4\,4}][PF_6]$

system has slightly higher CO_2 uptake than $[P_{6\,4\,4\,4}][PF_6]$ with the same concentration. When the concentrations of ammonium and phosphonium ILs were larger than 1.25 wt %, the CO_2 capture capacity of phosphonium IL systems was much higher than those of ammonium ILs.

3.5. CO_2 Consumption Rates. Gas consumption rates are often used to characterize the rate of gas hydrate formation. Figure 9a−e shows the gas consumption rate kinetic curves of five IL systems with different concentrations in 0∼20 min under 2 MPa. The gas consumption in the first 20 min mainly depends on the CO_2 solubility of the IL mixed system, and in this period, all gas consumption rates are very close, reaching a range of 2.00−2.50 mmol CO_2/(mol H_2O·min).

In order to more explicitly identify the variation characteristics of gas consumption rates during the CO_2 hydrate growth process, the real-time gas consumption rate curves within 200−800 min under 2 MPa are shown in Figure 10a−e. In these figures, the changing trend of the gas consumption rate of each system is consistent, and a strong peak appears during the hydrate growth stage. As the hydration reaction weakens, the gas consumption rate gradually decreases until it tends to about 0.00 mmol CO_2/(mol H_2O·min).

Figure 10a−c respectively demonstrates the real-time CO_2 gas consumption rate kinetic curves of $[N_{2\,2\,2\,2}]Br$, $[N_{2\,2\,2\,2}]$-$[NTf_2]$, and $[N_{2\,2\,2\,2}][PF_6]$ systems with different concentrations. In Figure 10a, the peak value of the CO_2 consumption rate of the pure water system was 0.31 mmol CO_2/(mol H_2O·
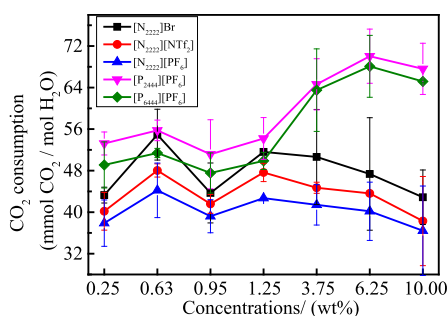

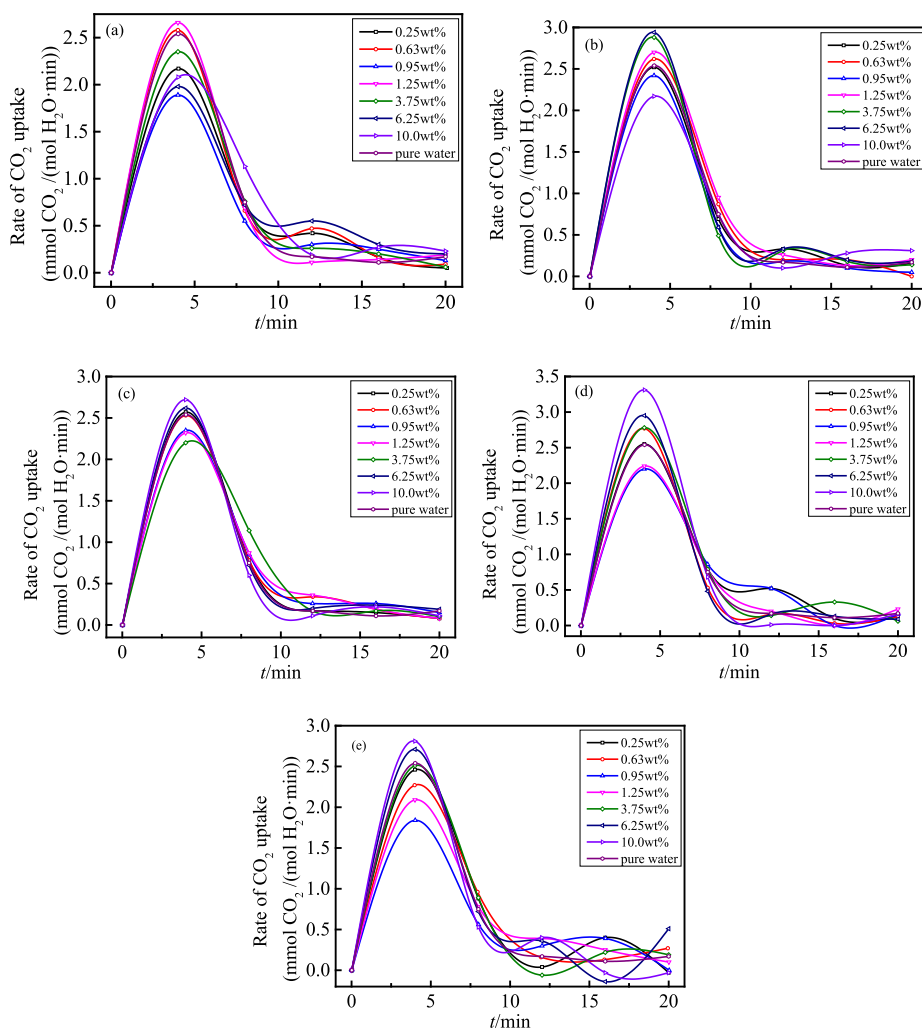**Figure 8.** Comparison chart of CO_2 gas consumption of five IL systems with different concentrations under 2 MPa.

Figure 9. Real-time CO_2 consumption rate curves in the presence of different IL concentration systems within 0~20 min under 2 MPa. (a) $[N_{2\,2\,2\,2}]Br$, (b) $[N_{2\,2\,2\,2}][NTf_2]$, (c) $[N_{2\,2\,2\,2}][PF_6]$, (d) $[P_{2\,4\,4\,4}][PF_6]$, and (e) $[P_{6\,4\,4\,4}][PF_6]$.

min), and the peak values of $[N_{2\,2\,2\,2}]Br$ systems were 0.13, 0.21, 0.17, 0.26, 0.50, 0.12, and 0.05 mmol $CO_2/$(mol $H_2O\cdot$ min) at 0.25, 0.63, 0.95, 1.25, 3.75, 6.25, and 10.00 wt %, respectively. It could be seen that except for the 3.75 wt % system, the peak values of the CO_2 consumption rate of the other $[N_{2\,2\,2\,2}]Br$ systems were lower than that of the pure water system, implying that $[N_{2\,2\,2\,2}]Br$ could reduce the CO_2 consumption rate and was not conducive to the growth of CO_2 hydrates. As observed in Figure 10b,c, the gas consumption rates of all $[N_{2\,2\,2\,2}][NTf_2]$ and $[N_{2\,2\,2\,2}][PF_6]$ systems were also lower than that of the pure water system during the hydrate growth phase, indicating that $[N_{2\,2\,2\,2}][NTf_2]$ and $[N_{2\,2\,2\,2}][PF_6]$ also made a kinetic inhibitory effect on the growth of CO_2 hydrates.

In Figure 10d, the peak values of the gas consumption rate in $[P_{2\,4\,4\,4}][PF_6]$ systems with concentrations of 0.25, 0.63, 0.95, 1.25, 3.75, 6.25, and 10.00 wt % were 0.14, 0.52, 0.26, 0.44, 0.42, 0.40, and 0.41 mmol $CO_2/$(mol $H_2O\cdot$min), respectively. Except for 0.25 and 0.95 wt % systems, $[P_{2\,4\,4\,4}][PF_6]$ with other concentrations could effectively enhance the gas consumption rate compared with the pure water system. As shown in Figure 10e, $[P_{6\,4\,4\,4}][PF_6]$ systems demonstrate similar gas consumption rate rules, indicating that adding

$[P_{2\,4\,4\,4}][PF_6]$ and $[P_{6\,4\,4\,4}][PF_6]$ made a kinetic promoting effect on the growth of CO_2 hydrates.

3.6. Water to Hydrate Conversion. Figure 11 shows the water to hydrate conversion of all IL experimental systems. Compared with the pure water system (27.56%), the systems with ILs had higher conversion. Combined with Table 2, the change rules of conversion with IL concentrations were consistent with gas consumption. In the ammonium ILs, conversion decreased with the increase of IL concentration except for 0.25 and 0.95 wt % systems. However, conversion roughly increased with the increasing concentration of $[P_{2\,4\,4\,4}][PF_6]$ and $[P_{6\,4\,4\,4}][PF_6]$. The conversion of ammonium IL systems at the same concentration was slightly different, and the influence order of anions on conversion followed $Br^- > [NTf_2]^- > [PF_6]^-$. Additionally, the $[P_{2\,4\,4\,4}][PF_6]$ systems had slightly higher conversion than $[P_{6\,4\,4\,4}][PF_6]$. When the concentrations of ammonium and phosphonium ILs were larger than 1.25 wt %, the conversion of phosphonium IL systems (45−50%) was much higher than those of ammonium ILs (30−40%).

4. INFLUENCE OF IL STRUCTURES

From the above experimental results, it is found that $[P_{2\,4\,4\,4}][PF_6]$ and $[P_{6\,4\,4\,4}][PF_6]$ ILs are generally more
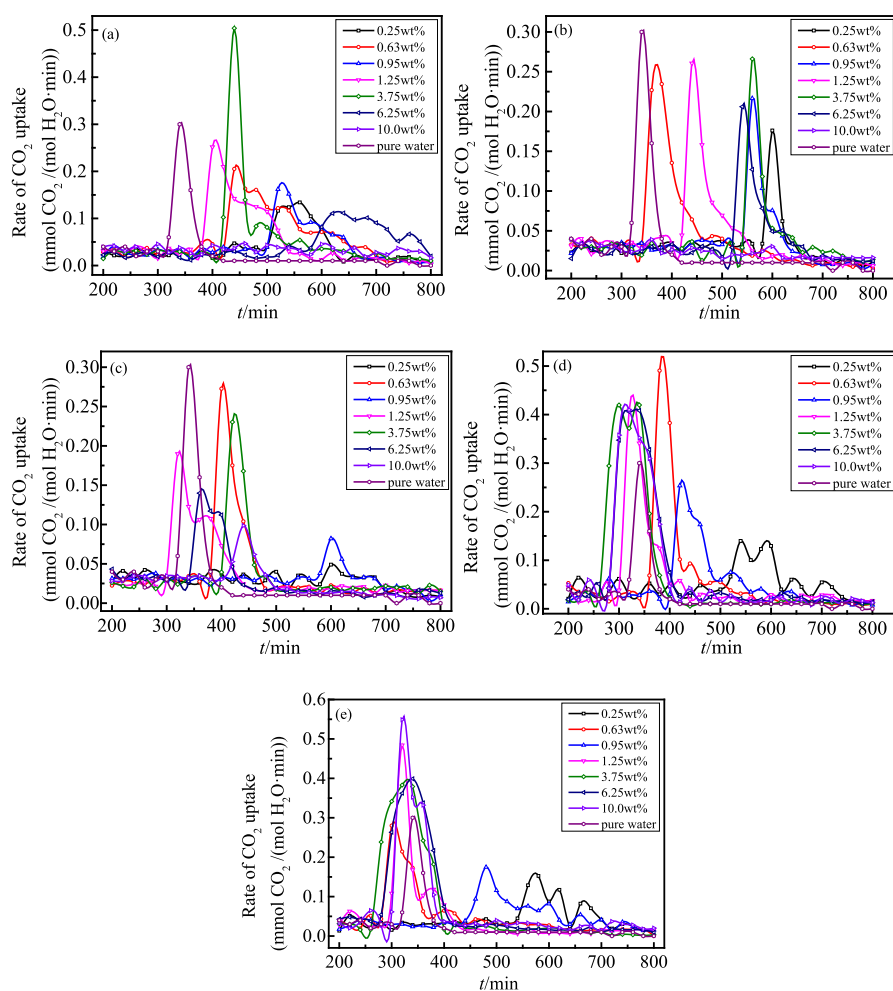
Figure 10. Real-time CO_2 consumption rate curves in the presence of different IL concentration systems within 200~800 min under 2 MPa. (a) $[N_{2\,2\,2\,2}]Br$, (b) $[N_{2\,2\,2\,2}][NTf_2]$, (c) $[N_{2\,2\,2\,2}][PF_6]$, (d) $[P_{2\,4\,4\,4}][PF_6]$, and (e) $[P_{6\,4\,4\,4}][PF_6]$.
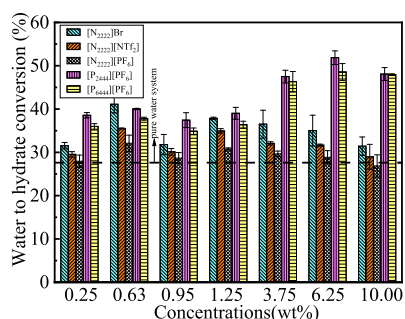

Figure 11. Water to hydrate conversion for CO_2 hydrate formation with different concentrations of ILs at 2 MPa.

favorable for improving CO_2 hydrates to create, kinetically increase CO_2 consumption, and fasten the hydrate growing rate compared to their ammonium congeners.

This may be due to the fact that the phosphonium and ammonium ILs have different charge distribution characteristics. It was reported that the P atom of the tetraalkylphosphonium-based IL cation is more positively charged than the N atom in the tetraalkylammonium-based analogous IL cation, and a noticeable charge delocalization occurred in the tetraalkylammonium cation, when compared with the respective phosphonium congener. This charge delocalization is responsible for the enhanced polarity observed on the

ammonium-based ILs, which leads to the stronger hydrogen bonding ability with water when more ammonium ILs were added. Overall, it is theoretically believable that the quaternary phosphonium ILs are better promoters while the ammonium ones performed inhibition effect.[58]

Another problem worthy to be noted is that $[N_{2\,2\,2\,2}]Br$ actually plays an inhibition role in CO_2 hydrate formation, which is distinctly different from the performance of its analogue counterpart $[N_{4\,4\,4\,4}]Br$. It was reported that $[N_{4\,4\,4\,4}]Br$ can form semi-clathrate hydrates under 0.1 MPa and 12 °C,[59,60] and small gas molecules can be trapped in the dodecahedral cavities (5^{12}) at favorable temperatures and pressures.[26,61] Adding $[N_{4\,4\,4\,4}]Br$ can alter the equilibrium to a lower pressure at a given temperature for CO_2 hydrates which indicates that $[N_{4\,4\,4\,4}]Br$ is a thermodynamics promoter for CO_2 hydrates.[25,59,62,63]

In order to investigate the differences of the effect of $[N_{2\,2\,2\,2}]Br$ and $[N_{4\,4\,4\,4}]Br$ on the formation of CO_2 hydrates, the interaction forces between anions and cations of $[N_{2\,2\,2\,2}]Br$ and $[N_{4\,4\,4\,4}]Br$ were calculated by Dmol. In addition, large-scale atomic/molecular massively parallel simulator (LAMMPS) molecular dynamics simulation was carried out to quantify the strength of interaction forces between molecules in different systems, and the radial distribution function (RDF) between molecules in the two systems was analyzed to explain the difference between the effects of
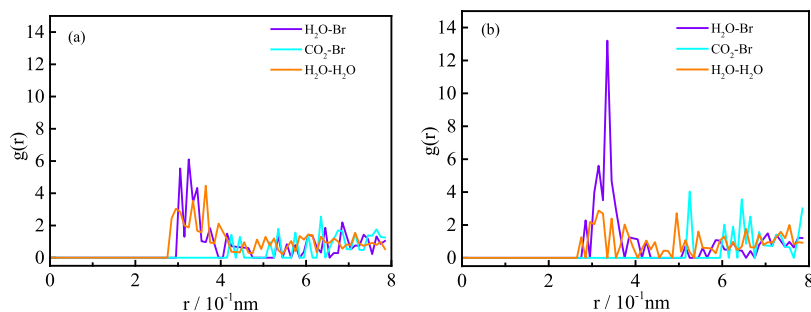
Figure 12. Radial distribution functions between the center of mass of H_2O molecules and Bromine atoms and between the center of mass of CO_2 molecules and Bromine atoms and between the center of mass of H_2O molecules in the two systems at 263 K under a pressure of 20 MPa, respectively. (a) $[N_{2\,2\,2\,2}]Br + H_2O + CO_2$ and (b) $[N_{4\,4\,4\,4}]Br + H_2O + CO_2$.

$[N_{2\,2\,2\,2}]Br$ and $[N_{4\,4\,4\,4}]Br$ on the formation of CO_2 hydrates from the microscopic scale.

4.1. Cation−Anion Interaction. From the reported mechanism of gas absorption in room-temperature ionic liquids, symmetric characteristics, alkyl chain length, polarity of ILs, and the size and quadrupole moments of gases make contributions to the sorption and selectivity.[64−67] In order to get a deep insight of the molecular reason for the above experimental results, quantum chemistry computations were conducted based on density functional theory (DFT). All these calculations were performed using the Dmol3 module of Material Studios, applying Grimme-corrected BLYP to describe the interaction between the cation and anion. All geometries were calculated with a complete optimization without any constraints at a basis set of DNP.

According to the Dmol3 calculation, the cation−anion intramolecular interaction force of $[N_{2\,2\,2\,2}]Br$ (−367.57 kJ/mol) is stronger than that of $[N_{4\,4\,4\,4}]Br$ (−341.32 kJ/mol). Therefore, the anion Br^- of $[N_{2\,2\,2\,2}]Br$ is difficult to crosslink with water molecules to form semi-clathrate hydrates compared to $[N_{4\,4\,4\,4}]Br$.

4.2. RDF Analysis. Molecular dynamics (MD) simulation provides a good way for the study of microscopic interactions between gas and water. The structures of the IL and CO_2 are optimized based on the DFT level, using the B3LYP/DNP (3.5) basis set in Dmol3. MD simulations are performed by the LAMMPS module of the Materials and Processes Simulations (MAPS) platform.[68] The amorphous structures were constructed using the MAPS platform with an initial structure size of 47 Å × 47 Å × 47 Å, and the density was set to be 1 g cm^{-3} (40 water molecules, 20 carbon dioxide molecules, and 10 IL molecules were randomly placed in the simulation). The time step used in the MD simulation process was set to be 1 fs, and the Nose−Hoover thermostat was applied to control the temperature and pressure.[69] The Ewald-summation method was set with a cut-off radius of 1.2 nm for the electrostatic interaction calculations. Long-range dispersion for van der Waals interactions was considered, and the dreiding_umbrella force field was applied. The energy minimization and annealing processes were performed on the system to obtain the reliable initial configurations on a basis of canonical ensemble (NVT) from 278.18 to 498 K and then 498 to 273 K. After annealing, the configuration with the lowest total energy was extracted for the further isothermal−isobaric (NPT) calculation with a running time of 2 ns at 263 K under a pressure of 20 MPa.

RDF[70] is a conditional probability density function for finding an atom at a distance, r, from a given atom located as the origin. RDF is normalized so that they approach unity as r approaches infinity. RDF is routinely used to characterize structure at the atomic level. Here, RDF was applied to characterize the ordered distribution of the interaction distances of anion−water, anion−CO_2, and water−water in $[N_{2\,2\,2\,2}]Br + H_2O + CO_2$ and $[N_{4\,4\,4\,4}]Br + H_2O + CO_2$ systems. The peak of RDF is high and sharp, indicating a strong order and close connection between atoms, as well as the strong interaction between molecules.

From the RDF diagram of $[N_{2\,2\,2\,2}]Br + H_2O + CO_2$ and $[N_{4\,4\,4\,4}]Br + H_2O + CO_2$ (Figure 12), it can be seen that the peak value of $g_{H2O−Br}(r)$ in the $[N_{4\,4\,4\,4}]Br + H_2O + CO_2$ system is significantly higher than that in the $[N_{2\,2\,2\,2}]Br + H_2O + CO_2$ system. This indicates that the strength of interaction force between Br^- and water in the $[N_{4\,4\,4\,4}]Br + H_2O + CO_2$ system is high, which is due to the participation of Br^- in the formation of semi-clathrate hydrates. In addition, the first peak of $g_{H2O−Br}(r)$ in the $[N_{4\,4\,4\,4}]Br + H_2O + CO_2$ system is located at 2.85 Å, which may be caused by hydrogen bonds formed between water molecules and Br^- anions, forming the semi-clathrate hydrates where the water molecules together with Br^- build a polyhedral host framework of the cages.[61,71,72] In comparison, the first peak of $g_{H2O−Br}(r)$ is located at 3.05 Å with weak interaction force between H_2O and Br^-, indicating that Br^- is less likely to participate in the formation of cages in the $[N_{2\,2\,2\,2}]Br + H_2O + CO_2$ system.

Besides, it is clearly seen that the first peak of $CO_2−Br^-$ of the $[N_{2\,2\,2\,2}]Br + H_2O + CO_2$ system appeared earlier than that of the $[N_{4\,4\,4\,4}]Br + H_2O + CO_2$ system, and the $[N_{2\,2\,2\,2}]Br + H_2O + CO_2$ system has more peaks than the $[N_{4\,4\,4\,4}]Br + H_2O + CO_2$ system. This indicates that in the $[N_{2\,2\,2\,2}]Br + H_2O + CO_2$ system, there are many interacting sites between CO_2 and Br^-, which means that Br^- anions are relatively more dispersed. However, the $[N_{4\,4\,4\,4}]Br + H_2O + CO_2$ system has fewer $CO_2−Br$ peaks due to the engagement of Br^- in hydrate cages, leading to limited sites for $CO_2−Br^-$ interaction. This also confirms that Br^- in $[N_{2\,2\,2\,2}]Br$ is less likely to participate in the creation of cages. The longer first peak of $CO_2−Br^-$ also may be due to a fact that for the semi-clathrate hydrates in the presence of $[N_{4\,4\,4\,4}]Br$, $[N_{4\,4\,4\,4}]^+$ will be incorporated as a guest molecule which competes with CO_2.[61,71,72]

In addition, the first peak of $g_{H2O−H2O}(r)$ in the $[N_{4\,4\,4\,4}]Br + H_2O + CO_2$ system locates at 2.75 Å, which corresponds to the distance between the O atoms of the hydrogen-bonded water molecules.[73] A shorter distance indicates a stronger hydrogen bond, and a higher peak means a larger probability of hydrogen bond formation between water molecules. The strong interaction forces between water molecules are favorable for adjusting the distance and angle between water molecules to

create hydrogen bonds which are required for cage structures[74] and then attracting CO_2 molecules through the hydrogen bond net structures. In comparison, the first peak of $g_{H2O-H2O}(r)$ in the $[N_{2\,2\,2\,2}]Br + H_2O + CO_2$ system locates at 2.95 Å, indicating that a weaker hydrogen bonding strength. Furthermore, the higher probability of H_2O-H_2O hydrogen bonding in $[N_{2\,2\,2\,2}]Br + H_2O + CO_2$ implies a less possibility of creating semi-clathrate hydrates involving Br^-.

5. CONCLUSIONS

The phase equilibrium temperatures, induction times, CO_2 consumptions and consumption rates, and water to hydrate conversions of CO_2 hydrates were studied under 2 MPa in the presence of $[N_{2\,2\,2\,2}]Br$, $[N_{2\,2\,2\,2}][NTf_2]$, $[N_{2\,2\,2\,2}][PF_6]$, $[P_{2\,4\,4\,4}][PF_6]$, and $[P_{6\,4\,4\,4}][PF_6]$ with concentrations of 0.25, 0.63, 0.95, 1.25, 3.75, 6.25, and 10.00 wt %.

All five ILs could increase CO_2 consumption and enhance the water to hydrate conversion. $[P_{2\,4\,\,4}][PF_6]$ and $[P_{6\,4\,4\,4}][PF_6]$ shifted the phase equilibrium temperature of CO_2 hydrates to a slightly higher temperature and shortened the induction time, showing their dual function promotion effects. $[N_{2\,2\,2\,2}]Br$, $[N_{2\,2\,2\,2}][NTf_2]$, and $[N_{2\,2\,2\,2}][PF_6]$ made the dual thermodynamics−kinetics inhibition effects. The inhibition effects of anions on CO_2 hydrates follow an order of $Br^- > [NTf_2]^- > [PF_6]^-$, which shows that $[N_{2\,2\,2\,2}]Br$ is the most promising dual hydrate inhibitor.

According to DFT and MD calculations, it is found that the anion−cation interaction in $[N_{2\,2\,2\,2}]Br$ is stronger than that in $[N_{4\,4\,\,4}]Br$, which may lead to the weakening of the interaction between the anion and water for $[N_{2\,2\,2\,2}]Br$. The results of RDF show that in the $[N_{4\,4\,4}]Br + H_2O + CO_2$ system, the hydrogen bonding force between water and Br^- is obviously stronger than that in the $[N_{2\,2\,2\,2}]Br + H_2O + CO_2$ system. Therefore, the Br^- anion of $[N_{2\,2\,2\,2}]Br$ is less likely to crosslink with water molecules to form semi-clathrate hydrates, which may be the main reason for the different roles of $[N_{2\,2\,2\,2}]Br$ and $[N_{4\,4\,4}]Br$.

■ AUTHOR INFORMATION

Corresponding Authors

Yongliang Xu − *School of Safety Science and Engineering, Henan Polytechnic University, Jiaozuo 454003, China; Collaborative Innovation Center for Coal Safety Production & High-Efficient-Clean Utilization for Coal by Provincial and Ministerial Co-Construction, Jiaozuo 454003, China; State Key Laboratory Cultivation Base for Gas Geology and Gas Control in Henan Polytechnic University, Jiaozuo 454003, China;* orcid.org/0000-0001-5484-4952; Email: xylcumt@hpu.edu.cn

Yajuan Zhang − *College of Oceanography, Hohai University, Nanjing 210098, China;* Email: zhangyajuan000000@163.com

Authors

Lanyun Wang − *School of Safety Science and Engineering, Henan Polytechnic University, Jiaozuo 454003, China; Collaborative Innovation Center for Coal Safety Production & High-Efficient-Clean Utilization for Coal by Provincial and Ministerial Co-Construction, Jiaozuo 454003, China; State Key Laboratory Cultivation Base for Gas Geology and Gas Control in Henan Polytechnic University, Jiaozuo 454003, China*

Yu Chen − *School of Safety Science and Engineering, Henan Polytechnic University, Jiaozuo 454003, China*

Yao Li − *School of Safety Science and Engineering, Henan Polytechnic University, Jiaozuo 454003, China; Collaborative Innovation Center for Coal Safety Production & High-Efficient-Clean Utilization for Coal by Provincial and Ministerial Co-Construction, Jiaozuo 454003, China; State Key Laboratory Cultivation Base for Gas Geology and Gas Control in Henan Polytechnic University, Jiaozuo 454003, China;* orcid.org/0000-0002-9342-1474

Yan Wang − *School of Safety Science and Engineering, Henan Polytechnic University, Jiaozuo 454003, China; Collaborative Innovation Center for Coal Safety Production & High-Efficient-Clean Utilization for Coal by Provincial and Ministerial Co-Construction, Jiaozuo 454003, China; State Key Laboratory Cultivation Base for Gas Geology and Gas Control in Henan Polytechnic University, Jiaozuo 454003, China;* orcid.org/0000-0001-6671-4661

Jianping Wei − *School of Safety Science and Engineering, Henan Polytechnic University, Jiaozuo 454003, China; Collaborative Innovation Center for Coal Safety Production & High-Efficient-Clean Utilization for Coal by Provincial and Ministerial Co-Construction, Jiaozuo 454003, China; State Key Laboratory Cultivation Base for Gas Geology and Gas Control in Henan Polytechnic University, Jiaozuo 454003, China*

Tingxiang Chu − *School of Safety Engineering, North China Institute of Science and Technology, Beijing 101601, China*

Complete contact information is available at:
https://pubs.acs.org/10.1021/acsomega.2c06621

Notes

The authors declare no competing financial interest.

■ REFERENCES

(1) Quéré, C. L.; Raupach, M. R.; Canadell, J. G.; Marland, G. Trends in the sources and sinks of carbon dioxide. *Nat. Geosci.* **2009**, *2*, 831−836.

(2) Metz, B.; Davidson, O.; Coninck, H. D.; Loos, M.; Meyer, L. *IPCC special report on carbon dioxide capture and storage*; Cambridge Univ Press: New York, 2005.

(3) Yu, D.; Wu, M.; Zhao, L.; Wang, Y. Research on Carbon Dioxide Capture and Storage Technology. *Contemp. Chem. Ind.* **2014**, *43*, 544−546. +549

(4) Bai, F.; Liu, N. Research Progress on Impact Mechanisms of Additives on CO_2 Hydrate Formation. *Chin. J. Refrig. Technol.* **2017**, *37*, 20−24. 31

(5) Qiang, W. Research Progress of Separation Experiment of Mine Gas Hydrate. *Coal Sci. Technol.* **2014**, *42*, 81−85.

(6) Yang, X.; Liu, H.; Li, Y. Research progress of separation technology based on hydrate formation. *CIESC J.* **2017**, *68*, 831−840.

(7) Peng, H.; He, H.; Wang, X. K.; Li, Y. Research Progress of the Exploitation of Natural Gas Hydrate With Carbon Dioxide Replacement Method. *Contemp. Chem. Ind.* **2019**, *48*, 170−174. +178

(8) Li, L.; Fan, S.; Wen, Y.; Li, Q.; Chen, Q. Hydrate based gas separation technology for CH_4/CO_2 mixtures:a review. *Chem. Ind. Eng. Prog.* **2018**, *37*, 4596−4605.

(9) Sloan, Jr, E. D.; Koh, C. A.*Clathrate Hydrates of Natural Gases.* Third ed.; CRC Press: Boca Raton, 2008.

(10) Adisasmito, S.; Frank, R. J., III; Sloan, E. D., Jr. Hydrates of Carbon Dioxide and Methane Mixtures. *J. Chem. Eng. Data* **1991**, *36*, 68−71.

(11) Servio, P.; Lagers, F.; Peters, C.; Englezos, P. Gas hydrate phase equilibrium in the system methane−carbon dioxide−neohexane and water. *Fluid Phase Equilib.* **1999**, *158-160*, 795−800.

(12) Li, X.-S.; Xu, C.-G.; Chen, Z.-Y.; Cai, J. Synergic effect of cyclopentane and tetra-n-butyl ammonium bromide on hydrate-based carbon dioxide separation from fuel gas mixture by measurements of gas uptake and X-ray diffraction patterns. *Int. J. Hydrogen Energy* **2012**, *37*, 720−727.

(13) Li, X.-S.; Xu, C.-G.; Chen, Z.-Y.; Wu, H.-J. Tetra-n-butyl ammonium bromide semi-clathrate hydrate process for post-combustion capture of carbon dioxide in the presence of dodecyl trimethyl ammonium chloride. *Energy* **2010**, *35*, 3902−3908.

(14) Ricaurte, M.; Dicharry, C.; Broseta, D.; Renaud, X.; Torré, J.-P. CO_2 Removal from a $CO_2−CH_4$ Gas Mixture by Clathrate Hydrate Formation Using THF and SDS as Water-Soluble Hydrate Promoters. *Ind. Eng. Chem. Res.* **2012**, *52*, 899−910.

(15) Ricaurte, M.; Torré, J.-P.; Asbai, A.; Broseta, D.; Dicharry, C. Experimental Data, Modeling, and Correlation of Carbon Dioxide Solubility in Aqueous Solutions Containing Low Concentrations of Clathrate Hydrate Promoters: Application to $CO_2−CH_4$ Gas Mixtures. *Ind. Eng. Chem. Res.* **2012**, *51*, 3157−3169.

(16) Earle, M. J.; Seddon, K. R.; Adams, C. J.; Roberts, G. Friedel−Crafts reactions in room temperature ionic liquids. *Chem. Commun.* **1998**, *19*, 2097−2098.

(17) Li, J. M.; Wang, S. L.; Rao, Y. C.; Zhang, L.; Dai, Y.; Liu, M. F. Experimental study on carbon dioxide hydrate formation strengthened by ionic liquid. *Mod. Chem. Ind.* **2014**, *34*, 124−127.

(18) Chen, Q.; Yu, Y.; Zeng, P.; Yang, W.; Liang, Q.; Peng, X.; Liu, Y.; Hu, Y. Effect of 1-butyl-3-methylimidazolium tetrafluoroborate on the formation rate of CO_2 hydrate. *J. Nat. Gas Chem.* **2008**, *17*, 264−267.

(19) Shin, J.-Y.; Kim, K.; Kang, S.-P.; Mun, S. Study on the Promotion Effect of Ionic Liquid on CH_4 Hydrate Formation. *Korean Chem. Eng. Res.* **2013**, *51*, 500−505.

(20) Kim, S.; Baek, I.-H.; You, J.-K.; Seo, Y. Guest gas enclathration in tetra-n-butyl ammonium chloride (TBAC) semiclathrates: Potential application to natural gas storage and CO_2 capture. *Appl. Energy* **2015**, *140*, 107−112.

(21) Zheng, J.; Zhang, P.; Linga, P. Semiclathrate hydrate process for pre-combustion capture of CO_2 at near ambient temperatures. *Appl. Energy* **2017**, *194*, 267−278.

(22) Shi, L.; Liang, D. Semiclathrate hydrate phase behaviour and structure for CH_4 in the presence of tetrabutylammonium fluoride (TBAF). *J. Chem. Thermodyn.* **2019**, *135*, 252−259.

(23) Sun, Z.-G.; Sun, L. Equilibrium Conditions of Semi-Clathrate Hydrate Dissociation for Methane + Tetra-n-butyl Ammonium Bromide. *J. Chem. Eng. Data* **2010**, *55*, 3538−3541.

(24) Lin, W.; Delahaye, A.; Fournaison, L. Phase equilibrium and dissociation enthalpy for semi-clathrate hydrate of CO_2+TBAB. *Fluid Phase Equilib.* **2008**, *264*, 220−227.

(25) Li, S.; Fan, S.; Wang, J.; Lang, X.; Wang, Y. Semiclathrate Hydrate Phase Equilibria for CO_2 in the Presence of Tetra-n-butyl Ammonium Halide (Bromide, Chloride, or Fluoride). *J. Chem. Eng. Data* **2010**, *55*, 3212−3215.

(26) Arjmandi, M.; Chapoy, A.; Tohidi, B. Equilibrium data of hydrogen, methane, nitrogen, carbon dioxide, and natural gas in semi-clathrate hydrates of tetra-butyl ammonium bromide. *J. Chem. Eng. Data* **2007**, *52*, 2153−2158.

(27) Magnusson, C. D.; Kelland, M. A. Study on the Synergistic Properties of Quaternary Phosphonium Bromide Salts with N-Vinylcaprolactam Based Kinetic Hydrate Inhibitor Polymers. *Energy Fuels* **2014**, *28*, 6803−6810.

(28) Li, X.-S.; Zhan, H.; Xu, C.-G.; Zeng, Z.-Y.; Lv, Q.-N.; Yan, K.-F. Effects of Tetrabutyl-(ammonium/phosphonium) Salts on Clathrate Hydrate Capture of CO_2 from Simulated Flue Gas. *Energy Fuels* **2012**, *26*, 2518−2527.

(29) Mayoufi, N.; Dalmazzone, D.; Furst, W.; Delahaye, A.; Fournaison, L. CO_2 Enclathration in Hydrates of Peralkyl-(Ammonium/Phosphonium) Salts: Stability Conditions and Dissociation Enthalpies. *J. Chem. Eng. Data* **2010**, *55*, 1271−1275.

(30) Nashed, O.; Sabil, K. M.; Lal, B.; Ismail, L.; Jaafar, A. J. Study of 1-(2-Hydroxyethyle) 3-methylimidazolium Halide as Thermodynamic Inhibitors. *Appl. Mech. Mater.* **2014**, *625*, 337−340.

(31) Tariq, M.; Connor, E.; Thompson, J.; Khraisheh, M.; Atilhan, M.; Rooney, D. Doubly dual nature of ammonium-based ionic liquids for methane hydrates probed by rocking-rig assembly. *RSC Adv.* **2016**, *6*, 23827−23836.

(32) Khan, M. S.; Bavoh, C. B.; Partoon, B.; Lal, B.; Bustam, M. A.; Shariff, A. M. Thermodynamic effect of ammonium based ionic liquids on CO_2 hydrates phase boundary. *J. Mol. Liq.* **2017**, *238*, 533−539.

(33) Marsh, K. N.; Deer, A.; Wu, A. C.-T.; Tran, E.; Klamt, A. Room Temperature Ionic Liquids as Replacements for Conventional Solvents - A Review. *Korean J. Chem. Eng.* **2002**, *19*, 357−362.

(34) Seddon, K. R.; Stark, A.; Torres, M.-J. Influence of chloride, water, and organic solvents on the physical properties of ionic liquids. *Pure Appl. Chem.* **2000**, *72*, 2275−2287.

(35) Xiao, C.; Adidharma, H. Dual function inhibitors for methane hydrate. *Chem. Eng. Sci.* **2009**, *64*, 1522−1527.

(36) Haruo, N. Solid-Liquid and Liquid-Liquid Phase Equilibria in the Symmetrical Tetraalkylammonium Halide−Water Systems. *Bull. Chem. Soc. Jpn.* **1981**, *54*, 3717−3722.

(37) Li, A.; Jiang, L.; Tang, S. An experimental study on carbon dioxide hydrate formation using a gas-inducing agitated reactor. *Energy* **2017**, *134*, 629−637.

(38) Fakharian, H.; Ganji, H.; Naderi Far, A.; Kameli, M. Potato starch as methane hydrate promoter. *Fuel* **2012**, *94*, 356−360.

(39) Peng, D.-Y.; Robinson, D. B. A New Two-Constant Equation of State. *Ind. Eng. Chem. Fundam.* **1976**, *15*, 59−64.

(40) Munck, J.; Skjold-Jørgensen, S.; Rasmussen, P. Computations of the formation of gas hydrates. *Chem. Eng. Sci.* **1988**, *43*, 2661−2672.

(41) Parrish, W. R.; Prausnitz, J. M. Dissociation Pressures of Gas Hydrates Formed by Gas Mixtures. *Ind. Eng. Chem. Process Des. Dev.* **1972**, *11*, 26−35.

(42) Mohammadi, A.; Manteghian, M.; Haghtalab, A.; Mohammadi, A. H.; Rahmati-Abkenar, M. Kinetic study of carbon dioxide hydrate formation in presence of silver nanoparticles and SDS. *Chem. Eng. J.* **2014**, *237*, 387−395.

(43) Vitu, S.; Jaubert, J.-N.; Pauly, J.; Daridon, J.-L.; Barth, D. Bubble and Dew Points of Carbon Dioxide + a Five-Component Synthetic Mixture: Experimental Data and Modeling with the PPR78 Model. *J. Chem. Eng. Data* **2007**, *52*, 1851−1855.

(44) Yu, Y.-S.; Zhou, S.-D.; Li, X.-S.; Wang, S.-L. Effect of graphite nanoparticles on CO_2 hydrate phase equilibrium. *Fluid Phase Equilib.* **2016**, *414*, 23−28.

(45) Seo, Y.-T.; Lee, H. Multiple-phase hydrate equilibria of the ternary carbon dioxide, methane, and water mixtures. *J. Phys. Chem. B* **2001**, *105*, 10084−10090.

(46) Shin, B. S.; Kim, E. S.; Kwak, S. K.; Lim, J. S.; Kim, K.-S.; Kang, J. W. Thermodynamic inhibition effects of ionic liquids on the formation of condensed carbon dioxide hydrate. *Fluid Phase Equilib.* **2014**, *382*, 270−278.

(47) Xiao, C.; Wibisono, N.; Adidharma, H. Dialkylimidazolium halide ionic liquids as dual function inhibitors for methane hydrate. *Chem. Eng. Sci.* **2010**, *65*, 3080−3087.

(48) Chu, C.-K.; Lin, S.-T.; Chen, Y.-P.; Chen, P.-C.; Chen, L.-J. Chain length effect of ionic liquid 1-alkyl-3-methylimidazolium chloride on the phase equilibrium of methane hydrate. *Fluid Phase Equilib.* 2016, 413, 57−64.

(49) Ye, N.; Zhang, P. Equilibrium Data and Morphology of Tetra-n-butyl Ammonium Bromide Semiclathrate Hydrate with Carbon Dioxide. *J. Chem. Eng. Data* 2012, 57, 1557−1562.

(50) Wang, X.; Dennis, M. Phase equilibrium and formation behaviour of CO_2 -TBAB semi-clathrate hydrate at low pressures for cold storage air conditioning applications. *Chem. Eng. Sci.* 2016, 155, 294−305.

(51) Wang, X.; Dennis, M. Phase Equilibrium and Formation Behavior of the CO_2−TBPB Semiclathrate Hydrate for Cold Storage Applications. *J. Chem. Eng. Data* 2017, 62, 1083−1093.

(52) Shi, L.-L.; Liang, D.-Q.; Li, D.-L. Phase Equilibrium Data of Tetrabutylphosphonium Bromide Plus Carbon Dioxide or Nitrogen Semiclathrate Hydrates. *J. Chem. Eng. Data* 2013, 58, 2125−2130.

(53) Mayoufi, N.; Dalmazzone, D.; Delahaye, A.; Clain, P.; Fournaison, L.; Fürst, W. Experimental Data on Phase Behavior of Simple Tetrabutylphosphonium Bromide (TBPB) and Mixed CO_2 + TBPB Semiclathrate Hydrates. *J. Chem. Eng. Data* 2011, 56, 2987−2993.

(54) Lü, R.; Lin, J.; Lu, Y.; Liu, D. The comparison of cation−anion interactions of phosphonium- and ammonium-based ionic liquids − A theoretical investigation. *Chem. Phys. Lett.* 2014, 597, 114−120.

(55) Jacquemin, J.; Husson, P.; Padua, A. A. H.; Majer, V. Density and viscosity of several pure and water-saturated ionic liquids. *Green Chem.* 2006, 8, 172−180.

(56) Swatloski, R. P.; Visser, A. E.; Reichert, W. M.; Broker, G. A.; Farina, L. M.; Holbrey, J. D.; Rogers, R. D. On the solubilization of water with ethanol in hydrophobic hexafluorophosphate ionic liquids. *Green Chem.* 2002, 4, 81−87.

(57) Olivier-Bourbigou, H.; Magna, L.; Morvan, D. Ionic liquids and catalysis: Recent progress from knowledge to applications. *Appl. Catal. A Gen.* 2010, 373, 1−56.

(58) Carvalho, P. J.; Ventura, S. P.; Batista, M. L.; Schroder, B.; Goncalves, F.; Esperanca, J.; Mutelet, F.; Coutinho, J. A. Understanding the impact of the central atom on the ionic liquid behavior:phosphonium vs ammonium cations. *J. Chem. Phys.* 2014, 140, No. 064505.

(59) Oyama, H.; Shimada, W.; Ebinuma, T.; Kamata, Y.; Takeya, S.; Uchida, T.; Nagao, J.; Narita, H. Phase diagram, latent heat, and specific heat of TBAB semiclathrate hydrate crystals. *Fluid Phase Equilib.* 2005, 234, 131−135.

(60) Dyadin, Y. A.; Udachin, K. A. Clathrate formation in water−peralkylonium salts systems. *J. Incl. Phenom.* 1984, 2, 61−72.

(61) Shimada, W.; Shiro, M.; Kondo, H.; Takeya, S.; Oyama, H.; Ebinuma, T.; Narita, H. Tetra-n-butylammonium bromide-water (1/38). *Acta Crystallogr., Sect. C: Cryst. Struct. Commun.* 2005, 61, o65−o66.

(62) Komatsu, H.; Hayasaka, A.; Ota, M.; Sato, Y.; Watanabe, M.; Smith, R. L., Jr. Measurement of pure hydrogen and pure carbon dioxide adsorption equilibria for THF clathrate hydrate and tetra-n-butyl ammonium bromide semi-clathrate hydrate. *Fluid Phase Equilib.* 2013, 357, 80−85.

(63) Joshi, A.; Sangwai, J. S.; Das, K.; Sami, N. A. Experimental investigations on the phase equilibrium of semiclathrate hydrates of carbon dioxide in TBAB with small amount of surfactant. *Int. J. Energy Environ. Eng.* 2013, 4, 1−8.

(64) Cardoso, P. F.; Fernandez, J.; Lepre, L. F.; Ando, R. A.; Costa Gomes, M. F.; Siqueira, L. J. A. Molecular dynamics simulations of polyethers and a quaternary ammonium ionic liquid as CO_2 absorbers. *J. Chem. Phys.* 2018, 148, 134908.

(65) Seyedhosseini, B.; Izadyar, M.; Housaindokht, M. R. A Computational Exploration of H_2S and CO_2 Capture by Ionic Liquids Based on alpha-Amino Acid Anion and N_7,N_9-Dimethyladeninium Cation. *J. Phys. Chem. A* 2017, 121, 4352−4362.

(66) Shi, W.; Maginn, E. J. Molecular simulation and regular solution theory modeling of pure and mixed gas absorption in the ionic liquid 1-n-hexyl-3-methylimidazolium bis-(triflfluoromethylsulfonyl)amide (hmim Tf_2N). *J. Phys. Chem. B* 2008, 112, 16710−16720.

(67) Velarde, M. V.; Gallo, M.; Alonso, P. A.; Miranda, A. D.; Dominguez, J. M. DFT study of the energetic and noncovalent interactions between imidazolium ionic liquids and hydrofluoric acid. *J. Phys. Chem. B* 2015, 119, 5002−5009.

(68) Plimpton, S. Fast parallel algorithms for short-range molecular dynamics. *J. Comput. Phys.* 1995, 117, 1−19.

(69) Evans, D. J.; Holian, B. L. The Nose−Hoover thermostat. *J. Chem. Phys.* 1985, 83, 4069−4074.

(70) Cladek, B. R.; Everett, S. M.; McDonnell, M. T.; Tucker, M. G.; Keffer, D. J.; Rawn, C. J. Guest−Host Interactions in Mixed CH_4−CO_2 Hydrates: Insights from Molecular Dynamics Simulations. *J. Phys. Chem. C* 2018, 122, 19575−19583.

(71) Aladko, L. S.; Dyadin, Y. A.; Rodionova, T. V.; Terekhova, I. S. Clathrate Hydrates of Tetrabutylammonium and Tetraisoamylammonium Halides. *J. Struct. Chem.* 2002, 43, 990−994.

(72) Shin, K.; Cha, J. H.; Seo, Y.; Lee, H. Physicochemical properties of ionic clathrate hydrates. *Chem. − Asian J.* 2010, 5, 22−34.

(73) Dongre, H. J.; Thakre, N.; Palodkar, A. V.; Jana, A. K. Carbon Dioxide Hydrate Growth Dynamics and Crystallography in Pure and Saline Water. *Cryst. Growth Des.* 2020, 20, 7129−7140.

(74) Gou, Q.*Factors influencing the formation and decomposition of methane hydrate based on molecular dynamics simulation*; Master's Thesis : Southwest Petroleum University, 2019.